UDK 621.791.725:628.483
Original scientific article/Izvirni znanstveni članek

ISSN 1580-2949
Mater. Tehnol.

COMPARISON OF POWDER-BED FUSION, DIRECTED-ENERGY DEPOSITION AND HYBRID ADDITIVE MANUFACTURING OF Ti6Al4V COMPONENTS: MICROSTRUCTURE, CORROSION AND MECHANICAL PROPERTIES

PRIMERJAVA TEHNOLOGIJ SPAJANJA SELEKTIVNEGA LASERSKEGA TALJENJA, DIREKTNEGA LASERSKEGA NAVARJANJA IN HIBRIDNE ADITIVNE PROIZVODNJE Ti6Al4V KOMPONENT: MIKROSTRUKTURA, KOROZIJA IN MEHANSKE LASTNOSTI

Aleksandra Kocijan*, Simon Malej

Institute of Metals and Technology, Lepi pot 11, SI-1000 Ljubljana, Slovenia

Prejem rokopisa – received: 2025-03-14; sprejem za objavo – accepted for publication: 2025-03-19

doi:10.17222/mit.2024.1423

This study investigates the microstructure, corrosion resistance, and mechanical properties of Ti6Al4V components fabricated using powder-bed fusion (PBF), directed-energy deposition (DED), and hybrid additive manufacturing (HAM) for aerospace applications. To prevent α' martensite formation, the samples were subjected to heat treatment. The microstructure was characterized using optical microscopy (OM), scanning electron microscopy (SEM), and electron-backscatter diffraction (EBSD). Corrosion resistance was assessed through potentiodynamic polarization tests, and mechanical properties were evaluated using Vickers hardness measurements. The PBF sample exhibited a fine, homogeneous microstructure with crystal grains and α-laths, while the DED sample showed visible deposition layers, a larger crystal grain structure, and α-lamella. The increased hardness of the DED sample was attributed to its higher nitrogen content, which acts as a solid-solution strengthening agent. Although the DED sample displayed lower thermodynamic stability, it demonstrated superior kinetic corrosion resistance compared to both the PBF and HAM samples.

Keywords: additive manufacturing, Ti6Al4V, microstructure, corrosion, mechanical properties

Raziskava obravnava mikrostrukturne, korozijske in mehanske lastnosti komponent iz zlitine Ti6Al4V, izdelanih z uporabo tehnologij Selektivnega laserskega taljenja (PBF), direktnega navarjanja (DED) in hibridne aditivne proizvodnje (HAM) za letalske aplikacije. Vzorce smo toplotno obdelali, da bi preprečili nastanek α' martenzita. Mikrostrukturo smo ovrednotili z uporabo optične mikroskopije (OM), vrstične elektronske mikroskopije (SEM) in uklona povratno sipanih elektronov (EBSD). Korozijsko obstojnost smo preskušali z uporabo potenciodinamskih polarizacijskih testov, mehanske lastnosti pa z merjenjem trdote po Vickersu. Pri vzorcu PBF smo dokazali fino, homogeno mikrostrukturo s kristalnimi zrni in α-latami, medtem ko je vzorec DED pokazal vidne plasti navarjanja, večja kristalna zrna in α-lamele. Povečano trdoto vzorca DED smo pripisali večji vsebnosti dušika, ki deluje kot utrjevalec v trdni raztopini. Pri vzorcu DED smo opazili nižjo termodinamsko stabilnost, a hkrati višjo kinetično korozijsko odpornost v primerjavi z vzorcema PBF in HAM.

Ključne besede: dodajna tehnologija, Ti6Al4V, mikrostruktura, korozija, mehanske lastnosti

1 INTRODUCTION

The Ti6Al4V alloy is the most widely used titanium alloy due to its unique combination of high strength, low density, excellent fracture toughness, and outstanding corrosion resistance.[1] These properties make it particularly suitable for demanding applications in the aerospace, biomedical, and automotive industries.[1] Since the 1950s, Ti6Al4V has been a key material in aerospace engineering, where its high strength-to-weight ratio provides advantages in structural components.[2] However, despite its desirable properties, the alloy presents several challenges to conventional manufacturing due to its poor thermal conductivity, strain hardening, and high oxygen affinity.[3,4] Traditional manufacturing processes such as forging, casting, rolling, and machining not only require extensive material removal, but also lead to high production costs, material waste, and a longer manufacturing time.[5]

To overcome these limitations, additive manufacturing (AM) has emerged as a transformative technology for producing Ti6Al4V components.[6–9] AM offers several advantages over conventional methods, including design flexibility, material efficiency, and the ability to manufacture complex geometries with reduced lead times. Various AM techniques are available for metallic materials, with powder-bed fusion (PBF) and directed-energy deposition (DED) being the most commonly used for Ti6Al4V.[10,11] PBF technology enables the fabrication of high-precision parts with fine microstructural control, but it is relatively time consuming. DED, on the other

*Corresponding author's e-mail:
aleksandra.kocijan@imt.si (Aleksandra Kocijan)

hand, allows faster deposition rates and larger build volumes, although at the expense of dimensional accuracy and surface finish. Despite these benefits, AM also introduces specific challenges, including residual stresses, porosity, and surface roughness, all of which can influence the mechanical performance and corrosion behaviour of the final components.[12–16]

One of the key challenges in the AM of Ti6Al4V is the microstructural evolution due to the unique thermal conditions of the process.[17] Rapid melting resolidification and processing conditions like atmosphere during AM processing result in the formation of a non-equilibrium microstructure (like α' martensite), which is different to the α+β microstructure found in conventionally processed Ti6Al4V.[18] While α' martensite enhances strength, it compromises ductility and toughness, necessitating post-processing treatments such as heat treatment to refine the microstructure and optimize the mechanical properties. Studies have shown that a heat treatment above 700 °C can lead to complete decomposition of the α' martensite into a more stable α+β phase, improving the material´s ductility and toughness.[18–20]

In addition to mechanical properties, the corrosion resistance of AM Ti6Al4V is a crucial factor for aerospace applications.[21,22] The presence of α' martensite generally reduces the corrosion resistance compared to conventionally processed Ti6Al4V.[23] Heat treatment has been shown to enhance corrosion resistance by eliminating metastable phases and stabilizing the oxide layer on the alloy´s surface.[23] However, research on the electrochemical behaviour of AM Ti6Al4V remains limited, particularly concerning localised corrosion mechanisms. Surface-modification techniques such as plasma treatments can further improve the corrosion resistance by enhancing the quality and thickness of the oxide layer, while preserving the underlying microstructure.[24]

To fully exploit the advantages of AM, this study proposes a hybrid manufacturing approach, combining PBF and DED for the production of Ti6Al4V components for aerospace applications. This hybrid approach aims to leverage the precision and fine microstructural control of PBF, while benefiting from the high deposition rates of DED. However, integrating these two technologies introduces challenges related to the interface between the joined sections, where differences in microstructure, residual stresses, and thermal properties must be carefully managed. Process-parameter optimization, post-processing heat treatments, and surface finishing therefore play a crucial role in ensuring that the final component meets the rigorous mechanical and corrosion-resistance requirements of aerospace applications.

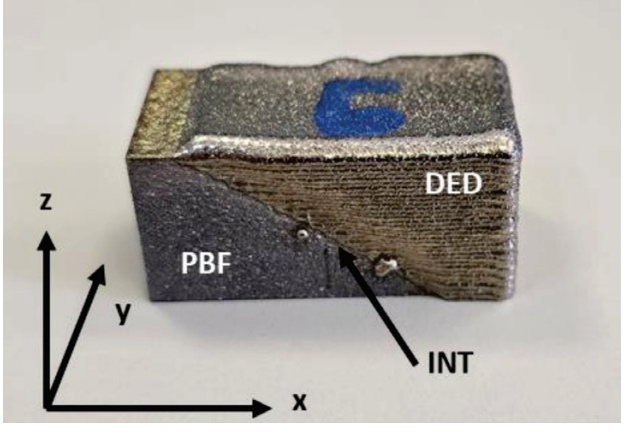

Figure 1: Photograph of finished HAM sample build by PBF and DED technology in a process chain. The INT (interface) with a black arrow shows the interface between the PBF and DED technology.

2 EXPERIMENTAL

Praxair (Indianapolis, USA) supplied the powder for the PBF and DED processes. The PBF and DED parts were built on the base plate, which was machined from Ti6Al4V. The HAM samples were built in two stages.[25] The first stage was the PBF process, where an edge-shaped object was built with an inclination of 35°. In the second stage, partially on the base plate and partially on the inclined PBF surface, Ti6Al4V was deposited by the DED process. The final dimension of the test sample was a block with dimensions of (30 × 15 × 15) mm (**Figure 1**). The PBF parts were processed by Trumpf TruPrint 3000 (DISTECH GmbH, Kapfenberg, Austria). The DED samples were made by OPTOMEC 850R LENS machine at BALMAR d.o.o. and EMO Orodjarna d.o.o. (Celje, Slovenia). The PBF and DED process parameters are listed in **Table 1**, and the build direction for both processes is the z axis. After processing, the samples were heat treated in a laboratory high-temperature resistance furnace at 800°C for 2h and furnace cooled to room temperature to prevent α' martensite formation. The chemical analysis was made using Inductively Coupled Plasma Optical Electronic Spectroscopy (ICP-OES Agilent 5800 VDV) and ELTRA Elementrac ONH (to determine nitrogen, oxygen and hydrogen). The chemical analysis was made separately for the PBF and DED parts (**Table 2**). The DED parts showed an elevated N content exceeding ASTM F2924 – 14 standard (**Table 2**) as a result of a lower-quality atmosphere during processing.

Samples for microstructural examination were cut in the middle to see the ZX plane and ground and finally polished by OP-S (Suspension of silica particles) for SEM imaging. Samples for OM (Optical Microscopy) were etched using Krol's etch to expose the microstructure. The OM was conducted on a Carl Zeiss Imager.Z2m microscope. BEI (Backscattered-electron imaging) was conducted on a SEM (Scanning Electron Microscope) Thermo Scientific Apreo 2S. EBSD (Electron-Backscatter Diffraction) was conducted with a Carl Zeiss Cross Beam 550 SEM with EDAX Hikari Super EBSD camera, TEAM and OIM software. The Vickers hardness measurements were conducted on prepared samples for microstructural investigations on a FALCON

800G2/AO3. Three hardness profiles were measured to see the transition from the PBF to DED technology at the interface (INT).

Table 1: PBF and DED process parameters used in this investigation

Process	PBF	DED
Layer thickness, mm	0.03	0.3
Hatch spacing, mm	0.14	0.4
Laser feed rate, mm/min	1200	740
Laser power, W	280	450
Powder feed rate, min^{-1}	–	1.7
umHatch feed rate, %	–	140
Contour feed rate, %	–	50
Rotation angle, °	67	90

The test specimens were ground with SiC emery paper down to 1200 grit prior to the electrochemical studies, and then rinsed with distilled water. Potentiodynamic measurements were performed using a BioLogic® SP-300 instrument and EC-Lab® V11.27 software in a 3.5 % NaCl solution at room temperature for PBF-, DED- and HAM produced Ti6Al4V alloy. The electrochemical cell consisted of the investigated sample as a working electrode, an Ag/AgCl reference electrode (0.197 V vs. SHE) and a platinum-mesh counter electrode. Measurements were performed at a scan rate 1mV/s. Corrosion rates were calculated according to the ASTM G102-89 standard.[26]

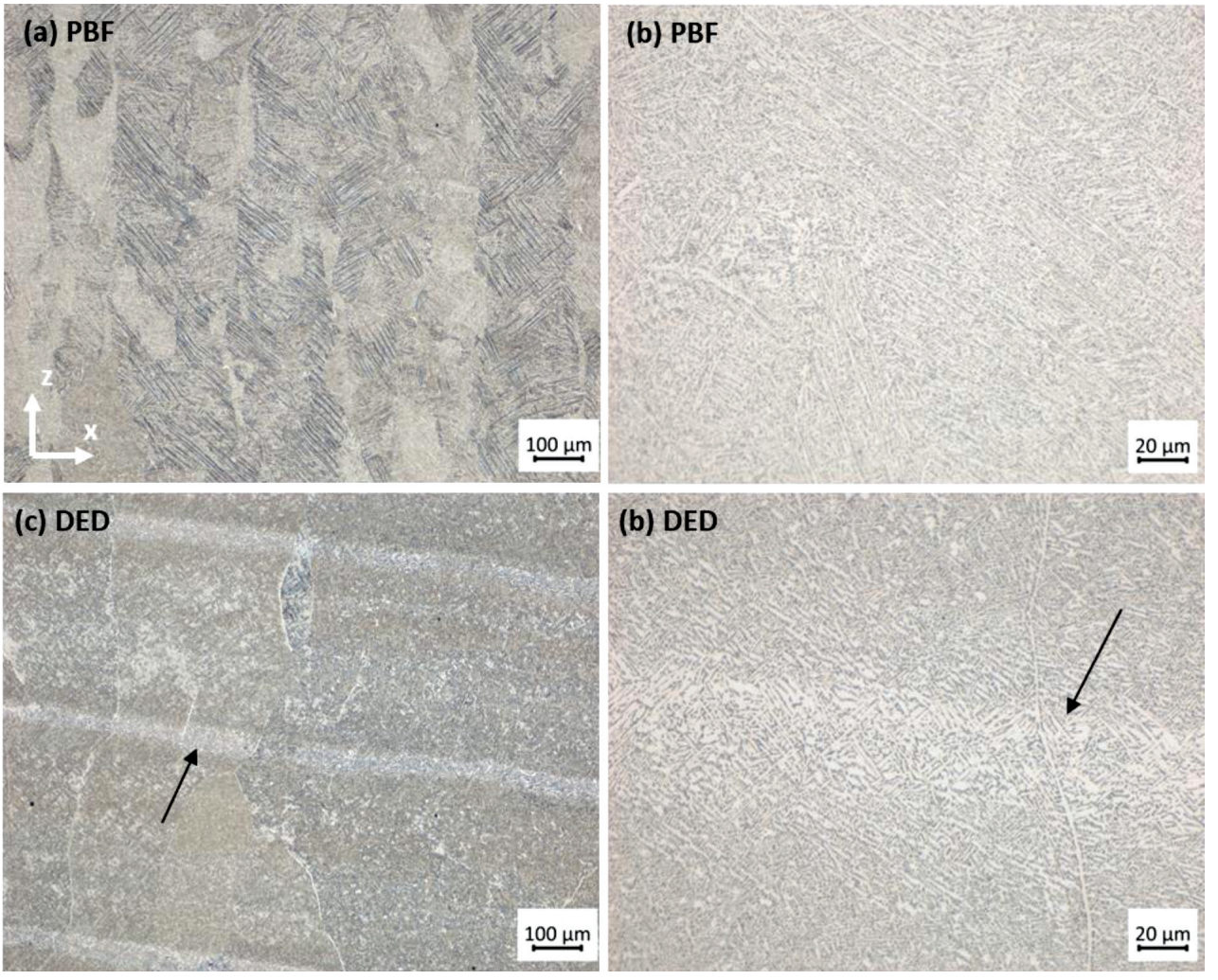

Figure 2: OM image of the microstructure in the (a and b) PBF and (c and d) DED part of the hybrid sample

Table 2: Average chemical composition of Ti6Al4V according to ASTM F2924-14 standard and analysis of as-processed PBF and DED samples

Standard/Process		H	N	O	C	Al	V	Fe	Ti
ASTM F2924 – 14	Min.	–	–	–	–	5.5	3.5	–	
	Max.	0.015	0.05	0.2	0.08	6.75	4.5	0.3	Balance
PBF		0.0046	0.025	0.170	0.032	5.5	3.7	0.14	Balance
DED		0.0037	0.49	0.13	0.031	5.7	3.7	0.07	Balance

3 RESULTS AND DISCUSSION

The microstructure heavily influences the hardness and corrosion properties; therefore, it is essential to characterise it. **Figure 2** shows an OM image of the microstructure in (a and b) the PBF and (c and d) the DED part of the hybrid sample after heat treatment. A fine and homogeneous microstructure of crystal grains and α-laths characterises the PBF part. The DED part has visible deposition layers (**Figure 2c**, black arrow), a microstructure composed of α-lamella and a larger columnar crystal grain structure. The microstructure of α-lamella inside the layer (**Figure 2d**, black arrow) is coarser than the microstructure between the layers. The layering occurs due to heating from the deposition of the next layer. Furthermore, due to the nitrogen diffusion at the surface, the α-phase is stabilised.[27] The influence of nitrogen on the as-built microstructure of the DED part was investigated in more detail in a previous article.[28] SEM-BEI was employed to see the microstructure of the Ti6Al4V processed by the PBF and DED after heat treatment in more detail. PBF parts show long, thin α-laths and brighter β phase at the borders of the α-laths. Such a microstructure formed due to the transformation of the as-built microstructure of α' to α+β. In the BEI, the β-phase appears brighter as it contains V, which is a β-stabilising element.[29] In contrast, the DED produced thicker and shorter α-lamella (**Figure 3a** and **3b**). Furthermore, the β-phase is thicker, especially at the triple points. Vickers hardness measurements were made for both the PBF and DED parts where the average Vickers hardness of the DED (442.5HV1) part is much larger than the PBF (367.1HV1) parts, despite the finer microstructure (**Table 3**). The main contribution to high hardness is the increased nitrogen content in the DED part (**Table 2**). The nitrogen, an interstitial element, increases the hardness of Ti by hindering the dislocation glide.[30]

Table 3: Average Vickers hardness HV1 of the PBF and DED part.

	PBF	DED
1.	362.6	441.4
2.	369.7	442.2
3.	369.1	443.8
Average	367.1 ± 3.2	442.5 ± 1.0

The OM image of the microstructure at the interface (INT) between PBF and DED (**Figure 4**) shows the difference between the coarser DED and the finer PBF microstructure. We also observed pores in the shape of wedges, which is characteristic of a lack of fusion porosity. This tells us that the energy density at the INT was insufficient to melt the PBF part and the previous DED layer. SEM-BEI was used to characterise the

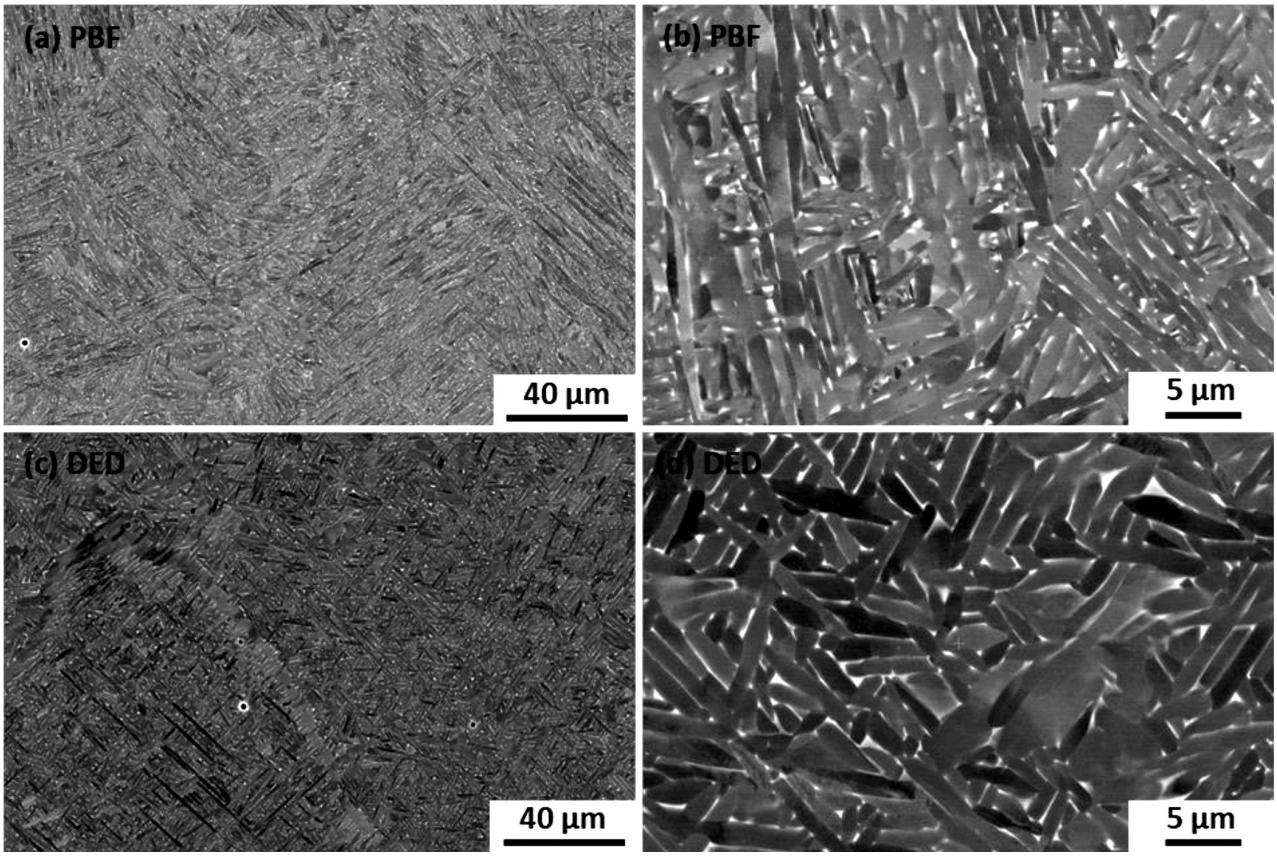

Figure 3: SEM-BEI of the microstructure in (a and b) PBF, (c and d) DED part of the HAM sample

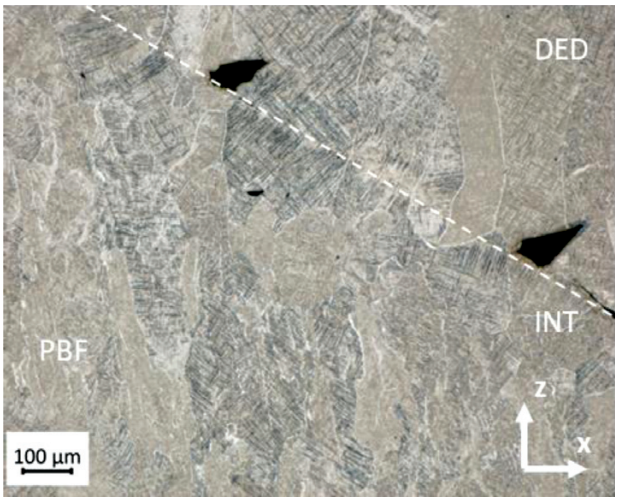

Figure 4: OM image of the microstructure at the INT between the PBF and DED technology of the HAM part

microstructure at the INT in more detail (**Figure 5a**). At the INT, there is a transition from finer grains to larger columnar grains with α_{GB} (α grain boundary) seen in **Figure 5b**, white arrows. With a slower cooling speed across β-transus temperature, α-phase can nucleate at the crystal grain borders.[31] Thus, the resulting microstructure contains a brighter phase semi-continuously distributed at the prior β grain boundaries. The orientation of the α_{GB} at the DED side of the INT is angled relative to the build direction (z-axis), almost 90° with respect to INT. The heat-conduction path is likely into the PBF part at the INT. Therefore, the β-grains at the INT during the DED deposition grew normal to the interface. This is a well-known phenomenon for the cubic-type crystal structure of the β phase (preferred grain growth direction is d).[32] There is no significant difference in the α-lamella size and shape of the PBF (**Figure 5c**) and DED sides (**Figure 5d**). A similar microstructure is expected since the PBF and DED parts near INT are exposed to a similar temperature cycle. At higher magnification, we can also see α_{GB} on the PBF side of the INT, in the HAZ (Heat Affected Zone (**Figure 5c**).

The prior-β grain scan is difficult to resolve completely with OM and SEM imaging. Therefore, we performed EBSD mapping of the (a) PBF, (b) DED and (c) INT area (**Figure 6**). We can see clearly that the prior-β grains are much larger in the DED part compared to the PBF. The difference is expected due to the lower cooling rate associated with the DED process.[33] A lower cooling rate enables the growth of larger columnar β grains and the formation of an α+β microstructure consisting of

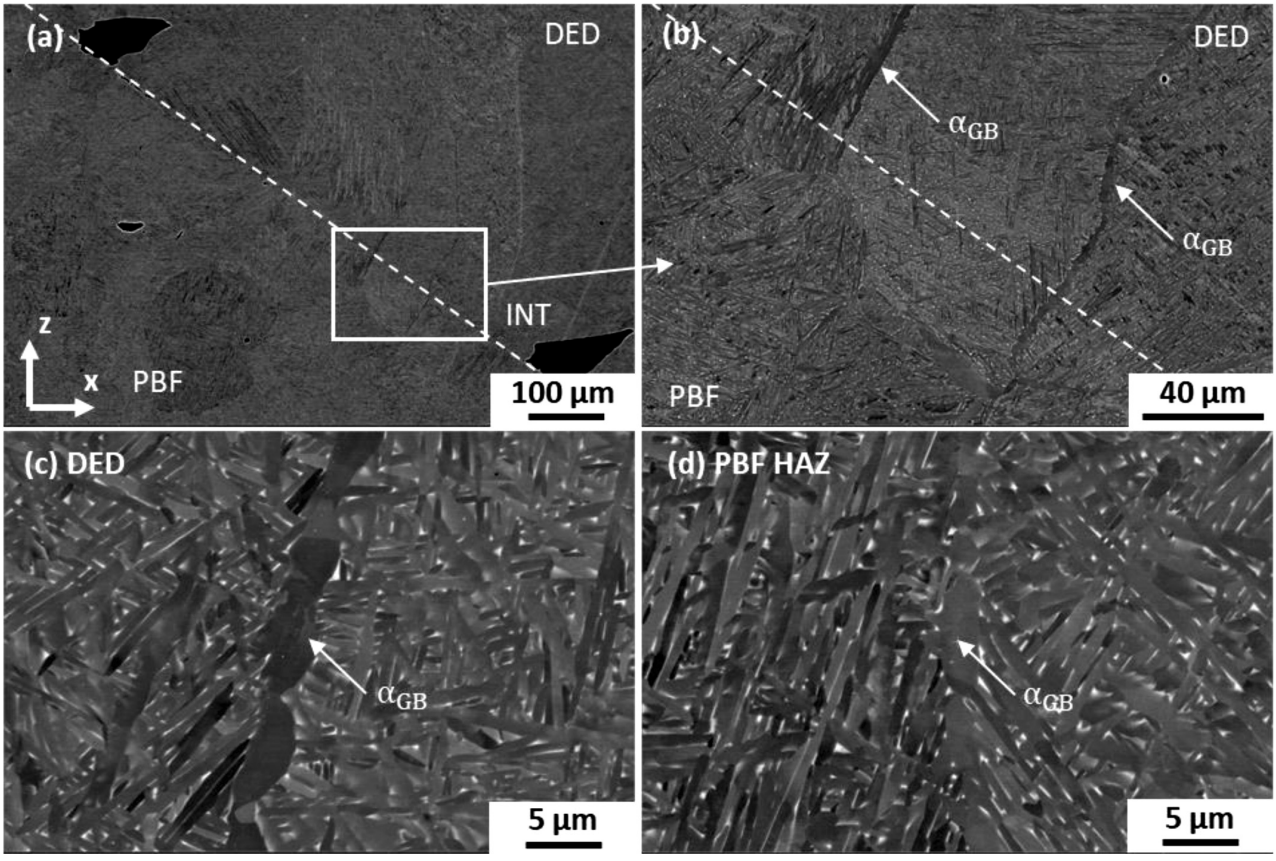

Figure 5: SEM-BEI of the microstructure at the INT between the PBF and DED technology (a) lack of fusion pores at the INT, (b) microstructure characteristics across the INT at 1000× magnification, (c) microstructure of HAZ in the PBF part and (d) microstructure of DED part close to the INT

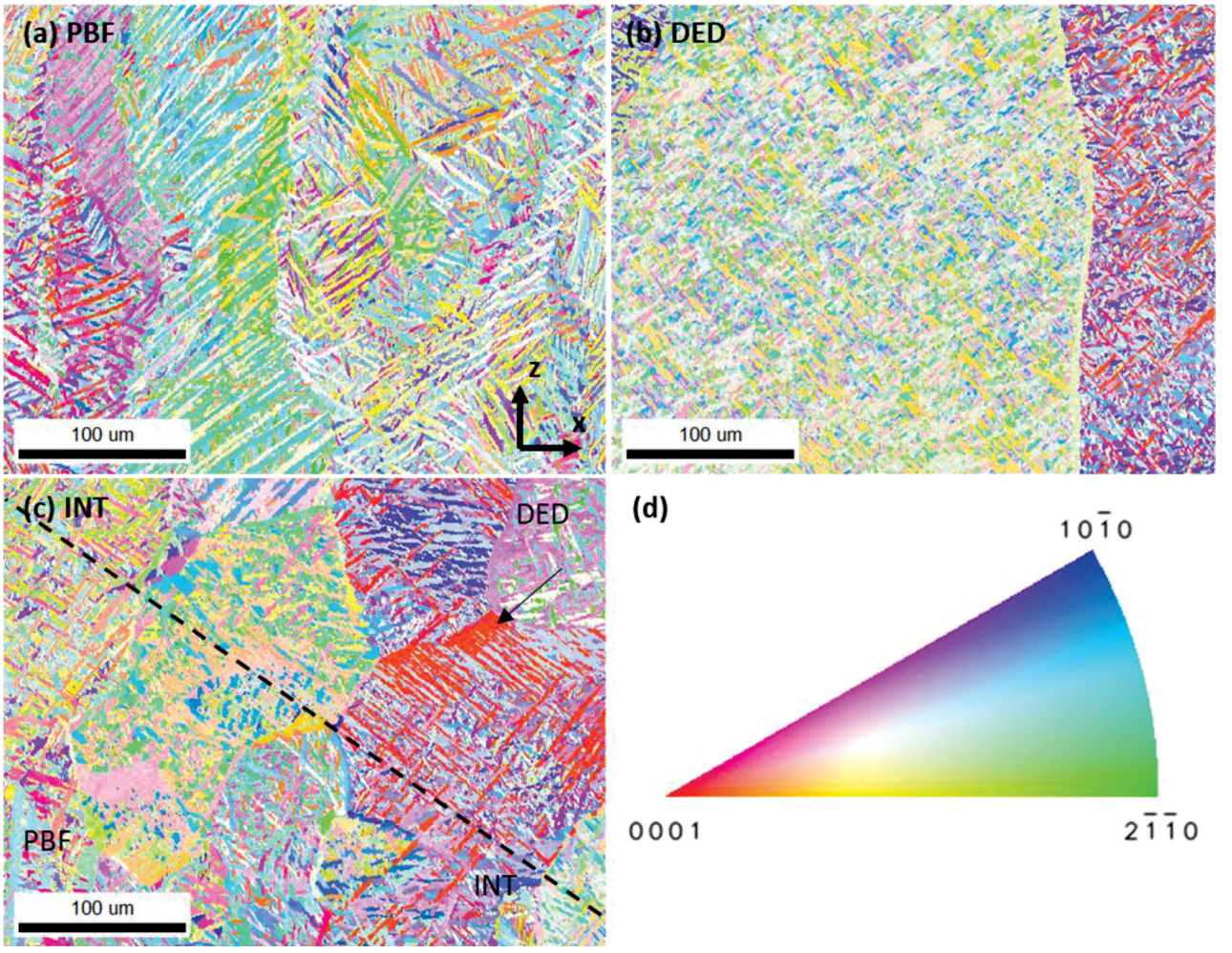

Figure 6: EBSD image of the (a) PBF, (b) DED (c) and INT part of the HAM sample. The dotted black line on (c) image show approximate location of the INT. The (d) image shows the inverse pole figure colour triangle for the α phase

α-lamella. At the INT, in addition to α-laths and α_{GB}, we also see lamella colonies of α-phase growing from the edge of prior β-grain boundary toward the centre of the grain. We can distinguish the colonies of α-phase since all the lamella show the same crystal orientation.[34] When the cooling rate is slow enough, the α-phase can nucleate at β-grain boundaries and form colonies.

The phase evolution is different at the interface than the bulk of the PBF and DED parts. Therefore, it is essential to see its influence on the hardness. We measured multiple Vickers hardness profiles normal to the INT (**Figure 7**). The Vickers hardness increases when transitioning from the PBF to the DED part. There is no change in the hardness of the PBF part close to the INT associated with the HAZ. The HAZ is smaller than the step size (0.5 mm), so it is undetected. Across the INT, we can see a large spread in the Vickers hardness for the DED part. We can see one or two maximums in each Vickers hardness profile. These maximums are associated with the layered microstructure of the DED part (**Figure 2b**). Due to nitrogen, the Vickers hardness is higher in the layer of coarse α+β microstructure than in the layers. The nitrogen is unevenly distributed across the thickness of each layer. More nitrogen was dissolved at the surface of the melt pool during the DED process than in the bulk due to the direct contact of the surface material with the atmosphere. Despite the partial shielding, a high content of N is still located in the layers since the Vickers hardness there is the same or higher than in

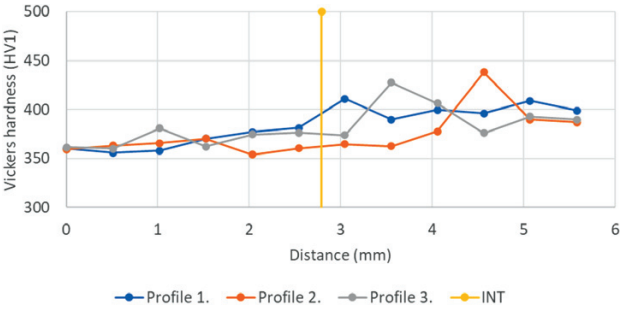

Figure 7: Vickers hardness profiles across the INT between the PBF and DED part. The PBF part present the left-hand side and the right-hand side DED part. Yellow line indicates the approximate location of the INT.

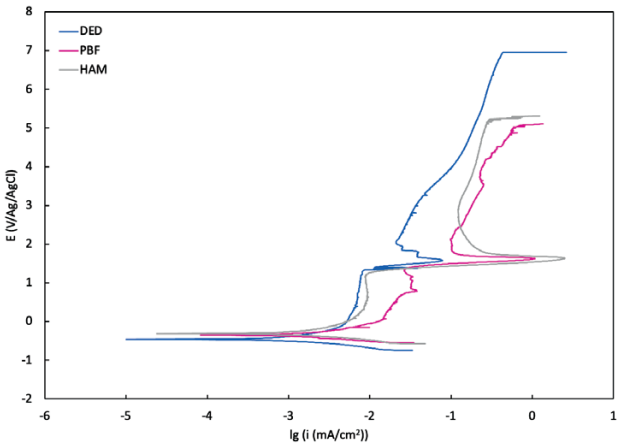

Figure 8: Potentiodynamic curves for DED, PBF and HAM Ti6Al4V alloy in 3.5 % NaCl solution.

the PBF part. While a high hardness is desirable in some applications, increased nitrogen is notorious for reducing the tensile and ductility properties.[28]

Table 4: Electrochemical parameters calculated from potentiodynamic curves for DED, PBF and HAM Ti6Al4V alloy in 3.5 % NaCl solution.

Sample	E_{corr} (mV)	i_{corr} (μA/cm^2)	v_{corr} (μm/year)
DED	–438.4	0.71	6.27
PBF	–371.3	0.99	8.71
HAM	–306.7	1.12	9.84

Potentiodynamic polarization measurements were used to evaluate the corrosion behaviour of DED, PBF and INT part of the HAM samples in 3.5 % NaCl solution (**Figure 8**). The electrochemical parameters determined from the potentiodynamic measurements, including corrosion potential (E_{corr}), corrosion current density (i_{corr}), and corrosion rate (v_{corr}), are summarized in the **Table 4**. Different manufacturing processing, such as DED, PBF, and HAM processes, can influence the microstructure, porosity, and residual stresses of metallic materials, ultimately affecting their corrosion resistance. Fine microstructures and higher densities generally enhance the corrosion resistance by minimizing the localized corrosion sites. Conversely, defects such as pores, inclusions, and grain-boundary segregation can accelerate corrosion.

However, the role of nitrogen in influencing the corrosion resistance is particularly important in this study. The nitrogen could enhance the corrosion resistance of the Ti6Al4V alloy by promoting the α-phase stabilisation, the formation of an oxide layer, improving passivation, and increasing the alloy's resistance to pitting and localized corrosion. The DED sample, despite having the most negative E_{corr}, exhibits the lowest i_{corr} and v_{corr}, indicating that it has a superior kinetic resistance to corrosion. This is also supported by its high breakdown potential (E_b) of 7 V vs. Ag/AgCl, which suggests a strong resistance to localized corrosion, such as pitting and crevice corrosion. The high E_b indicates that the surface of the DED part can withstand more aggressive corrosive environments before localized corrosion occurs.

In contrast, the PBF sample shows higher i_{corr} and v_{corr}, along with a lower E_b (5 V vs. Ag/AgCl), indicating a greater susceptibility to localized corrosion, despite possessing a finer microstructure. However, due to the increased energy density of the DED process, the resultant microstructure is more stable, as it was already partially annealed. Therefore, there are fewer lattice defects, which are known to impact corrosion resistance negatively. These defects were likely not completely removed from the PBF part with the chosen heat treatment. The lower nitrogen content at the surface of the PBF part could also be responsible for this increased vulnerability. Nitrogen can enhance the passive oxide layer, which enhances the corrosion resistance.[35] However, a more detailed investigation is needed to identify the mechanism when the content of N is low, with respect to other studies.

The INT area of the HAM sample, characterised by a lack of fusion pores, shows a similar trend in its corrosion behaviour, with higher i_{corr}, v_{corr}, and a lower E_b compared to the DED sample. The pores in the HAM sample may create weak points in the material, where corrosion can initiate more readily, thereby increasing its overall corrosion susceptibility.

4 CONCLUSIONS

This study highlights the influence of microstructural differences and nitrogen content on the corrosion and mechanical properties of Ti6Al4V alloy processed through different additive manufacturing techniques (PBF, DED and HAM):

The DED sample exhibits a coarser microstructure with larger prior-β grains and stabilized α-phase due to higher nitrogen content, while the PBF sample shows a finer, more homogeneous microstructure with smaller crystal grains and α-laths. The interface of the HAM sample displays increased pore formation, which affects its overall microstructure, corrosion resistance and hardness.

The DED sample has the highest Vickers hardness due to the increased nitrogen content, which strengthens the alloy by hindering dislocation glide. The PBF sample, with a finer microstructure, shows lower hardness than the DED part, likely due to the lower nitrogen content. The HAM sample, with defects such as pores, shows intermediate hardness, influenced by the microstructure and defects within the material.

The DED sample, characterized by a higher nitrogen content and coarser microstructure, demonstrates superior corrosion resistance compared to the PBF and HAM samples. The nitrogen-induced stabilization of the

α-phase in the DED part contributes to a more stable oxide layer, enhancing the protection against corrosion. Additionally, the increased energy density of the DED process results in a more stable microstructure, as it is partially annealed, leading to fewer lattice defects that typically reduce corrosion resistance. Despite having a finer microstructure, the PBF sample exhibits higher susceptibility to localized corrosion due to lower nitrogen content at its surface and lattice defects that were not fully eliminated during the chosen heat treatment. The HAM sample also exhibits higher corrosion rates due to defect formation, further compromising its corrosion resistance.

These findings emphasize the crucial role of material processing techniques in determining both mechanical properties and corrosion performance, especially in demanding applications. A comprehensive understanding of these factors is essential for selecting optimal materials and manufacturing methods for various environments, ultimately improving the durability and reliability of metallic components.

Data Availability

Data is available at Kocijan, Aleksandra; Malej, Simon (2025), "Dataset for a publication: "Comparison of Powder-Bed Fusion, Directed Energy Deposition, and Hybrid Additive Manufacturing of Ti6Al4V Components: Microstructure, Corrosion and Mechanical Properties"", Mendeley Data, V2, doi: 10.17632/4fmjjfpmyy.2.

Acknowledgments

This work was financially supported by the Slovenian Research Agency (Project No. L2-4445, core funding No. P2-0132 and infrastructure I0-0006).

5 REFERENCES

[1] C. Chunxiang, H. BaoMin, Z. Lichen, L. Shuangjin, Titanium alloy production technology, market prospects and industry development, Mater Des 32 (**2011**) 1684–1691. doi:10.1016/j.matdes.2010.09.011

[2] R. R. Boyer, An overview on the use of titanium in the aerospace industry, Materials science and engineering a-structural materials properties microstructure and processing 213 (**1996**) 103–114. doi:10.1016/0921-5093(96)10233-1

[3] C. de Formanoir, A. Brulard, S. Vives, G. Martin, F. Prima, S. Michotte, E. Riviere, A. Dolimont, S. Godet, A strategy to improve the work-hardening behavior of Ti-6Al-4V parts produced by additive manufacturing, Mater Res Lett 5 (**2017**) 201–208. doi:10.1080/21663831.2016.1245681

[4] L. Parry, I. A. Ashcroft, R.D. Wildman, Understanding the effect of laser scan strategy on residual stress in selective laser melting through thermo-mechanical simulation, Addit Manuf 12 (**2016**) 1–15. doi:10.1016/j.addma.2016.05.014

[5] R. Huang, M. Riddle, D. Graziano, J. Warren, S. Das, S. Nimbalkar, J. Cresko, E. Masanet, Energy and emissions saving potential of additive manufacturing: the case of lightweight aircraft components, J Clean Prod 135 (**2016**) 1559–1570. doi:10.1016/j.jclepro.2015.04.109

[6] M. Neikter, P. Akerfeldt, R. Pederson, M.-L. Antti, Microstructure characterisation of Ti-6Al-4V from different additive manufacturing processes, in: Mucklich, F and Bahre, D and Oden, M and Varna, J and Ayadi, Z and Anglada, M and Pierson, JF and Horwat, D (Ed.), International materials research meeting in the greater region: current trends in the characterisation of materials and surface modification, 2017. doi:10.1088/1757-899X/258/1/012007

[7] R. Hudak, M. Schnitzer, Z. O. Kralova, R. Gorejova, L. Mitrik, V. Rajtukova, T. Toth, M. Kovacevic, M. Riznic, R. Orinakova, J. Zivcak, Additive Manufacturing of Porous Ti6Al4V Alloy: Geometry Analysis and Mechanical Properties Testing, Applied sciences-Basel 11 (**2021**). doi:10.3390/app11062611

[8] S. Liu, Y.C. Shin, Additive manufacturing of Ti6Al4V alloy: A review, Mater Des 164 (**2019**). doi:10.1016/j.matdes.2018.107552

[9] A. Kushwaha, A. K. Subramaniyan, N. B. Kenchappa, S. Barad, Microstructure, mechanical, and wear properties of thin-walled Ti6Al4V parts produced using laser powder bed fusion technique, Mater Lett 308 (**2022**). doi:10.1016/j.matlet.2021.131138

[10] T. D. Ngo, A. Kashani, G. Imbalzano, K. T. Q. Nguyen, D. Hui, Additive manufacturing (3D printing): A review of materials, methods, applications and challenges, Compos B Eng 143 (**2018**) 172–196. doi:10.1016/j.compositesb.2018.02.012

[11] M. Godec, S. Malej, D. Feizpour, C. Donik, M. Balazic, D. Klobcar, L. Pambaguian, M. Conradi, A. Kocijan, Hybrid additive manufacturing of Inconel 718 for future space applications, Mater Charact 172 (**2021**). doi:10.1016/j.matchar.2020.110842

[12] C. Katinas, S. Liu, Y.C. Shin, Self-Sufficient Modeling of Single Track Deposition of Ti-6Al-4V With the Prediction of Capture Efficiency, Journal of manufacturing science and engineering-transactions of the ASME 141 (**2019**). doi:10.1115/1.4041423

[13] S. Liu, Y. C. Shin, Simulation and experimental studies on microstructure evolution of resolidified dendritic TiCx in laser direct deposited Ti-TiC composite, Mater Des 159 (**2018**) 212–223. doi:10.1016/j.matdes.2018.08.053

[14] K. Karolewska, B. Ligaj, M. Wirwicki, G. Szala, Strength analysis of Ti6Al4V titanium alloy produced by the use of additive manufacturing method under static load conditions, Journal of materials research and technology-JMR\&T 9 (**2020**) 1365–1379. doi:10.1016/j.jmrt.2019.11.063

[15] P.-H. Li, W.-G. Guo, W.-D. Huang, Y. Su, X. Lin, K.-B. Yuan, Thermomechanical response of 3D laser-deposited Ti-6Al-4V alloy over a wide range of strain rates and temperatures, Materials science and engineering a-structural materials properties microstructure and processing 647 (**2015**) 34–42. doi:10.1016/j.msea.2015.08.043

[16] E. Wycisk, A. Solbach, S. Siddique, D. Herzog, F. Walther, C. Emmelmann, Effects of Defects in Laser Additive Manufactured Ti-6Al-4V on Fatigue Properties, in: Schmidt, M and Vollertsen, F and Merklein, M (Ed.), 8th International conference on laser assisted net shape engineering (LANE 2014), 2014: pp. 371–378. doi:10.1016/j.phpro.2014.08.120

[17] K. Chang, E. Liang, W. Huang, X. Zhang, Y. Chen, J. Dong, R. Zhang, Microstructural feature and mechanical property in different building directions of additive manufactured Ti6Al4V alloy, Mater Lett 267 (**2020**). doi:10.1016/j.matlet.2020.127516

[18] G. Kasperovich, J. Hausmann, Improvement of fatigue resistance and ductility of TiAl6V4 processed by selective laser melting, J Mater Process Technol 220 (**2015**) 202–214. doi:10.1016/j.jmatprotec.2015.01.025

[19] D. Banerjee, J.C. Williams, Perspectives on Titanium Science and Technology, Acta Mater 61 (**2013**) 844–879. doi:10.1016/j.actamat.2012.10.043

[20] J. Yin, G. Peng, C. Chen, J. Yang, H. Zhu, L. Ke, Z. Wang, D. Wang, M. Ma, G. Wang, X. Zeng, Thermal behavior and grain growth orientation during selective laser melting of Ti-6Al-4V alloy, J Mater Process Technol 260 (**2018**) 57–65. doi:10.1016/j.jmatprotec.2018.04.035

[21] D.-I. Seo, J.-B. Lee, Corrosion Characteristics of Additive-Manufactured Ti-6Al-4V Using Microdroplet Cell and Critical Pitting Temperature Techniques, J Electrochem Soc 166 (**2019**) C428–C433. doi:10.1149/2.0571913jes

[22] W. Guo, H. Wang, P. Peng, B. Song, H. Zhang, T. Shao, H. Huan, H. Qiao, G. Qu, D. Zhu, J. Yan, Effect of laser shock processing on oxidation resistance of laser additive manufactured Ti6Al4V titanium alloy, Corros Sci 170 (**2020**). doi:10.1016/j.corsci.2020.108655

[23] N. Dai, J. Zhang, Y. Chen, L.-C. Zhang, Heat Treatment Degrading the Corrosion Resistance of Selective Laser Melted Ti-6Al-4V Alloy, J Electrochem Soc 164 (**2017**) C428–C434. doi:10.1149/2.1481707jes

[24] M. Mozetic, A. Vesel, G. Primc, C. Eisenmenger-Sittner, J. Bauer, A. Eder, G.H.S. Schmid, D.N. Ruzic, Z. Ahmed, D. Barker, K.O. Douglass, S. Eckel, J.A. Fedchak, J. Hendricks, N. Klimov, J. Ricker, J. Scherschligt, J. Stone, G. Strouse, I. Capan, M. Buljan, S. Milosevic, C. Teichert, S.R. Cohen, A.G. Silva, M. Lehocky, P. Humpolicek, C. Rodriguez, J. Hernandez-Montelongo, D. Mercier, M. Manso-Silvan, G. Ceccone, A. Galtayries, K. Stana-Kleinschek, I. Petrov, J.E. Greene, J. Avila, C.Y. Chen, B. Caja-Munoz, H. Yi, A. Boury, S. Lorcy, M.C. Asensio, J. Bredin, T. Gans, D. O'Connell, J. Brendin, F. Reniers, A. Vincze, M. Anderle, L. Montelius, Recent developments in surface science and engineering, thin films, nanoscience, biomaterials, plasma science, and vacuum technology, Thin Solid Films 660 (**2018**) 120–160. doi:10.1016/j.tsf.2018.05.046

[25] S. Malej, M. Godec, C. Donik, M. Balazic, R. Zettler, T. Lienert, L. Pambaguian, Hybrid additive manufacturing of Ti6Al4V with powder-bed fusion and direct-energy deposition, (**2023**). doi:10.1016/j.msea.2023.145229

[26] ASTM G102-89(2015)e1, Standard Practice for Calculation of Corrosion Rates and Related Information from Electrochemical Measurements, (2015)

[27] H. A. Wriedt, J. L. Murray, The N-Ti (Nitrogen-Titanium) system, Bulletin of Alloy Phase Diagrams 8 (**1987**) 378–388. doi:10.1007/BF02869274/METRICS

[28] S. Malej, Č. Donik, M. Balazic, M. Bizjak, M. Kač, M. Godec, Characterisation of the microstructure and defects during the direct energy deposition of hybrid ti6al4v in a low-quality atmosphere, Mater. Tehnol., 57 (**2023**) 209-216–209–216. doi:10.17222/MIT.2023.837

[29] L. Romero Resendiz, T. Sanchez Cano, M. Naeem, A. U. Rehman, E. Salamci, V. Torres Mendoza, E. Degalez Duran, L. Bazan Diaz, M.U. Salamci, Mechanical and Electrochemical Properties Comparison of Additively Manufactured Ti-6Al-4V Alloys by Electron Beam Melting and Selective Laser Melting, J Mater Eng Perform 33 (**2024**) 9028–9038. doi:10.1007/s11665-024-09486-4

[30] P. Vlcak, J. Drahokoupil, P. Vertat, J. Sepitka, J. Duchon, Hardness response to the stability of a Ti(+N) solid solution in an annealed TiN/Ti(+N)/Ti mixture layer formed by nitrogen ion implantation into titanium, J Alloys Compd 746 (**2018**) 490–495. doi:10.1016/J.JALLCOM.2018.02.301

[31] C. Liu, Y. Lu, X. Tian, D. Liu, Influence of continuous grain boundary α on ductility of laser melting deposited titanium alloys, Materials Science and Engineering: A 661 (**2016**) 145–151. doi:10.1016/J.MSEA.2016.03.034

[32] J. Li, X. Zhou, Q. Meng, M. Brochu, N. Chekir, J.J. Sixsmith, J.Y. Hascoët, Y.F. Zhao, Deterministic modeling of solidification microstructure formation in directed energy deposition fabricated Ti6Al4V, Addit Manuf 46 (**2021**) 102182. doi:10.1016/J.ADDMA.2021.102182

[33] A. Ty, Y. Balcaen, M. Mokhtari, J. Alexis, Influence of deposit and process parameters on microstructure and mechanical properties of Ti6Al4V obtained by DED-W (PAW), Journal of Materials Research and Technology 18 (**2022**) 2853–2869. doi:10.1016/J.JMRT.2022.03.169

[34] J. Chen, D. Fabijanic, M. Brandt, Y. Zhao, S. B. Ren, W. Xu, Dynamic α globularization in laser powder bed fusion additively manufactured Ti-6Al-4V, Acta Mater 255 (**2023**) 119076. doi:10.1016/J.ACTAMAT.2023.119076

[35] J. J. Velasco-Velez, B. Davaasuren, M. Scherzer, S. Cap, M. Willinger, J. H. Guo, R. Schlögl, A. Knop-Gericke, Exploring the incorporation of nitrogen in titanium and its influence on the electrochemical corrosion resistance in acidic media, Surf Sci 650 (**2016**) 272–278. doi:10.1016/J.SUSC.2016.01.007